Journal of Power Sources 196 (2011) 10112–10119

Contents lists available at SciVerse ScienceDirect

Journal of Power Sources

journal homepage: www.elsevier.com/locate/jpowsour

Microwave-assisted hydrothermal synthesis of transition-metal doped $ZnIn_2S_4$ and its photocatalytic activity for hydrogen evolution under visible light

Shaohua Shen*, Jie Chen, Xixi Wang, Liang Zhao, Liejin Guo*

State Key Laboratory of Multiphase Flow in Power Engineering, Xi'an Jiaotong University, Shaanxi 710049, China

ARTICLE INFO

Article history:
Received 1 June 2011
Received in revised form 24 August 2011
Accepted 24 August 2011
Available online 31 August 2011

Keywords:
Zinc indium sulfide
Transition metal
Photocatalytic
Hydrogen evolution

ABSTRACT

Aiming at the enhancement of photocatalytic activity for hydrogen evolution over $ZnIn_2S_4$, different transition metals (Cr, Mn, Fe, Co) are doped into the lattices of $ZnIn_2S_4$ to narrow the band gap. The doped $ZnIn_2S_4$ is characterized by XRD, Raman, UV–vis spectra, photoluminescence spectra, SEM and XPS techniques. The photocatalytic evaluation shows that Mn-doped $ZnIn_2S_4$ performs photocatalytic activity 20% higher than undoped $ZnIn_2S_4$, while Cr-, Fe-, and Co-doped $ZnIn_2S_4$ perform poorer activities in an order of Cr > Fe > Co. Based on the combined characterization results, the band structures of doped $ZnIn_2S_4$ are schematically depicted, which illustrates the different effects of transition-metal doping on the photocatalytic activity for hydrogen evolution. For Mn-doped $ZnIn_2S_4$, the enhancement of photocatalytic activity could be due to narrowed band gap induced by Mn doping. However, for Cr-, Fe-, and Co-doped $ZnIn_2S_4$, the suppressed photocatalytic activities should be attributed to the dopant-related impurity energy levels localizing the charge carriers or acting as non-radiative recombination centers for photoexcited electrons and holes. Hence, this study indicates that it is of great importance to make the in-depth investigation on the effects of band structures on the photocatalytic activity, especially for the doped semiconducting photocatalysts.

© 2011 Elsevier B.V. All rights reserved.

1. Introduction

Photocatalytic water splitting has been considered one of the most promising approaches to achieve the effective solar hydrogen conversion, since light-driven water splitting to hydrogen and oxygen was realized by Fujishima and Honda using semiconducting *n*-TiO_2 as anode and Pt as cathode to construct a photoelectrochemical cell [1]. Up to now, most photocatalysts can only split water under ultraviolet light irradiation, which occupies only 4% of the solar energy. For this reason, it is important to develop efficient photocatalysts capable of using ampler visible light, which occupies about 43% of the solar energy. In the past decades, different kinds of visible-light-active photocatalysts have been developed by various methods [2,3]. One effective method is to dope foreign metal ion into the parent semiconductor to expand its light absorption in visible light region.

In recent years, some multicomponent metal sulfides free of hypertoxic Cd^{2+} ions, such as Zn–In–S [4–7], Zn–In–Cu(Ag)–S [8–11], Cu(Ag)–In(Ga)–S [12–15], have been developed to show high photocatalytic activities under visible light. Among them, $ZnIn_2S_4$, as the only member of the AB_2X_4 family semiconductor with a layered structure, has attracted numerous interests, since Lei et al. [16] first treated $ZnIn_2S_4$ as an efficient visible-light-driven photocatalyst for hydrogen production. Thereafter, we found that the photocatalytic activity of $ZnIn_2S_4$ could be enhanced when hydrothermally prepared in the presence of cetyltrimethylammonium bromide (CTAB) [17,18]. In our following studies, the photocatalytic activity of CTAB-assisted hydrothermal synthesized $ZnIn_2S_4$ was further improved by loading transition-metal sulfides (CuS, Ag_2S) as oxidation-active cocatalysts [19] and doping transition-metal ions (Cu^{2+}, Ni^{2+}) to expand visible-light absorption range [20,21]. Thus, it is necessary to make a broad investigation on the transition-metal doped $ZnIn_2S_4$ photocatalysts and screen out the effective transition-metal dopants to improve the photocatalytic activity for hydrogen evolution.

Among the methods to prepare materials in mild conditions, microwave-assisted hydrothermal process was often found to have potential to enhance the crystallization kinetics of hydrothermal process and accelerate chemical reactions, thus leading to low energy consumption and time savings [22]. Herein, we used a microwave-assisted hydrothermal method to synthesize the transition-metal doped $ZnIn_2S_4$ (transition-metal, TM = Cr, Mn, Fe, Co) and investigated the doping effects of different transition-metal

* Corresponding author. Tel.: +86 29 82663895; fax: +86 29 82669033;.
E-mail addresses: shshen_xjtu@mail.xjtu.edu.cn (S. Shen), lj-guo@mail.xjtu.edu.cn (L. Guo).

0378-7753/$ – see front matter © 2011 Elsevier B.V. All rights reserved.
doi:10.1016/j.jpowsour.2011.08.103

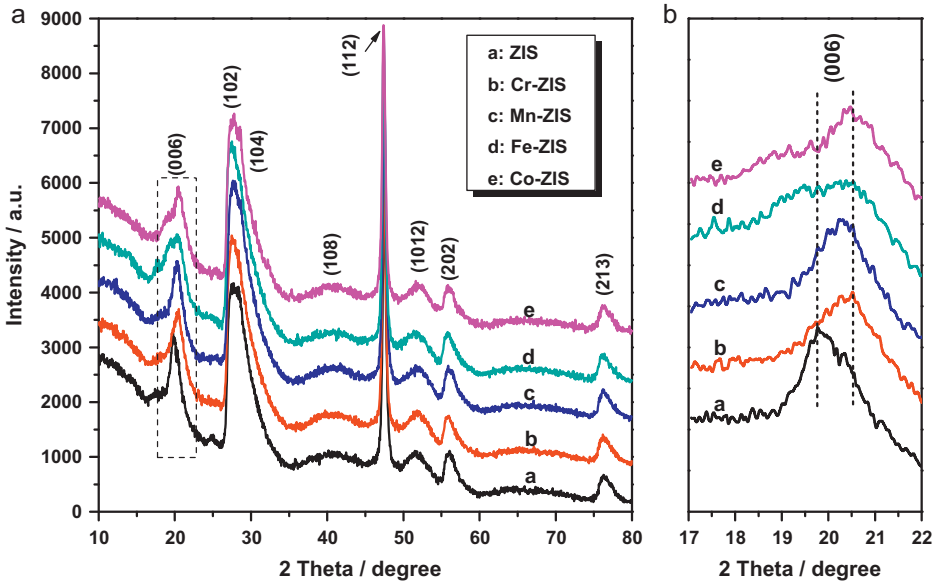

Fig. 1. XRD patterns of transition-metal doped $ZnIn_2S_4$ samples.

ions on the physicochemical properties, such as crystal structure and optical properties, and hence the photocatalytic activities for hydrogen evolution under visible light.

2. Experimental

2.1. Synthesis of transition-metal (Cr, Mn, Fe, Co) doped $ZnIn_2S_4$

All chemicals are of analytical grade and used as received without further purification. The doped $ZnIn_2S_4$ products were prepared by a microwave-assisted hydrothermal method. In a typical procedure, the stoichiometric amount of $ZnSO_4{\cdot}7H_2O$ and $InCl_3{\cdot}4H_2O$, 0.65 g of cetyltrimethylammonium bromide (CTAB) and a double excess of thioacetamide (TAA) were dissolved in 50 mL of distilled water. The mixed solution was transferred into a 100-mL Teflon-lined vessel, which was heated using microwave irradiation (CEM Mars microwave digestion system) to 160 °C for 1 h, and then cooled to room temperature naturally. A yellow precipitate was obtained, which was filtered and washed with absolute ethanol and distilled water for several times. $ZnIn_2S_4$ sample, labeled as ZIS, was obtained after dried at 80 °C. For synthesis of transition-metal (TM = Cr, Mn, Fe, Co) doped $ZnIn_2S_4$, a desired amount of $Cr(NO_3)_3$, $MnCl_2$, $FeCl_3$ and $Co(NO_3)_2$ aqueous solution was added into the mixed solution before microwave irradiation, respectively. The obtained transition-metal doped $ZnIn_2S_4$ photocatalysts were denoted as TM–ZIS (TM = Cr, Mn, Fe, Co).

2.2. Characterization

The X-ray diffraction (XRD) patterns were obtained from a PANalytical X'pert MPD Pro diffractometer using Ni-filtered Cu Kα irradiation (Wavelength 1.5406 Å). The X-ray photoelectron spectroscopy (XPS) measurements were conducted on a Kratos spectrometer (AXIS Ultra DLD) with monochromatic Al Kα radiation ($h\nu$ = 1486.69 eV) and with a concentric hemispherical analyzer. The diffuse reflection of the samples was determined by a Hitachi U-4100 UV–vis–near-IR spectrophotometer. Elemental Analysis was conducted on the Bruker S4 PIONEER X-ray fluorescence spectrum (XRF) using Rh target and maximum power of 4 kW. The sample morphology was observed by a JEOL JSM-6700FE scanning electron microscope. A Raman scattering study was performed on a Jobin Yvon LabRAM HR spectrometer using 514.5 nm irradiation from an argon ion laser at 20 mW.

2.3. Evaluation of photocatalytic activity

Photocatalytic hydrogen evolution was performed in a side irradiation Pyrex cell. A 500-W Xe lamp was used as the light source, and the UV part of the light was removed by a cut-off filter (λ > 430 nm). Hydrogen evolved was analyzed by an online thermal conductivity detector (TCD) gas chromatograph (NaX zeolite column, nitrogen as a carrier gas). In all experiments, 190 mL of deionized water containing 0.1 g of catalyst and 0.25 M Na_2SO_3/0.35 M Na_2S mixed sacrificial agent was added into the reaction cell. Here, sacrificial agent was used to scavenge photogenerated holes. Nitrogen was purged through the cell before reaction to remove oxygen. 1.0 wt% Pt as cocatalyst for the promotion of hydrogen evolution was photodeposited in situ on the photocatalyst from the precursor of $H_2PtCl_6{\cdot}6H_2O$. The temperature for all the photocatalytic reactions was kept at 35 °C. Control experiments

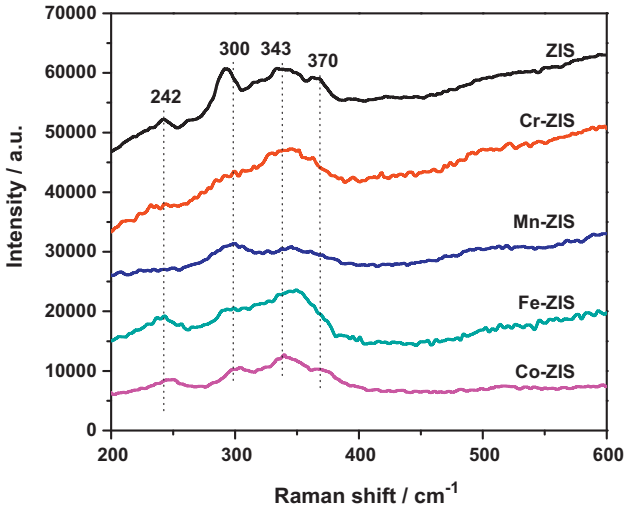

Fig. 2. Raman spectra of transition-metal doped $ZnIn_2S_4$ samples.

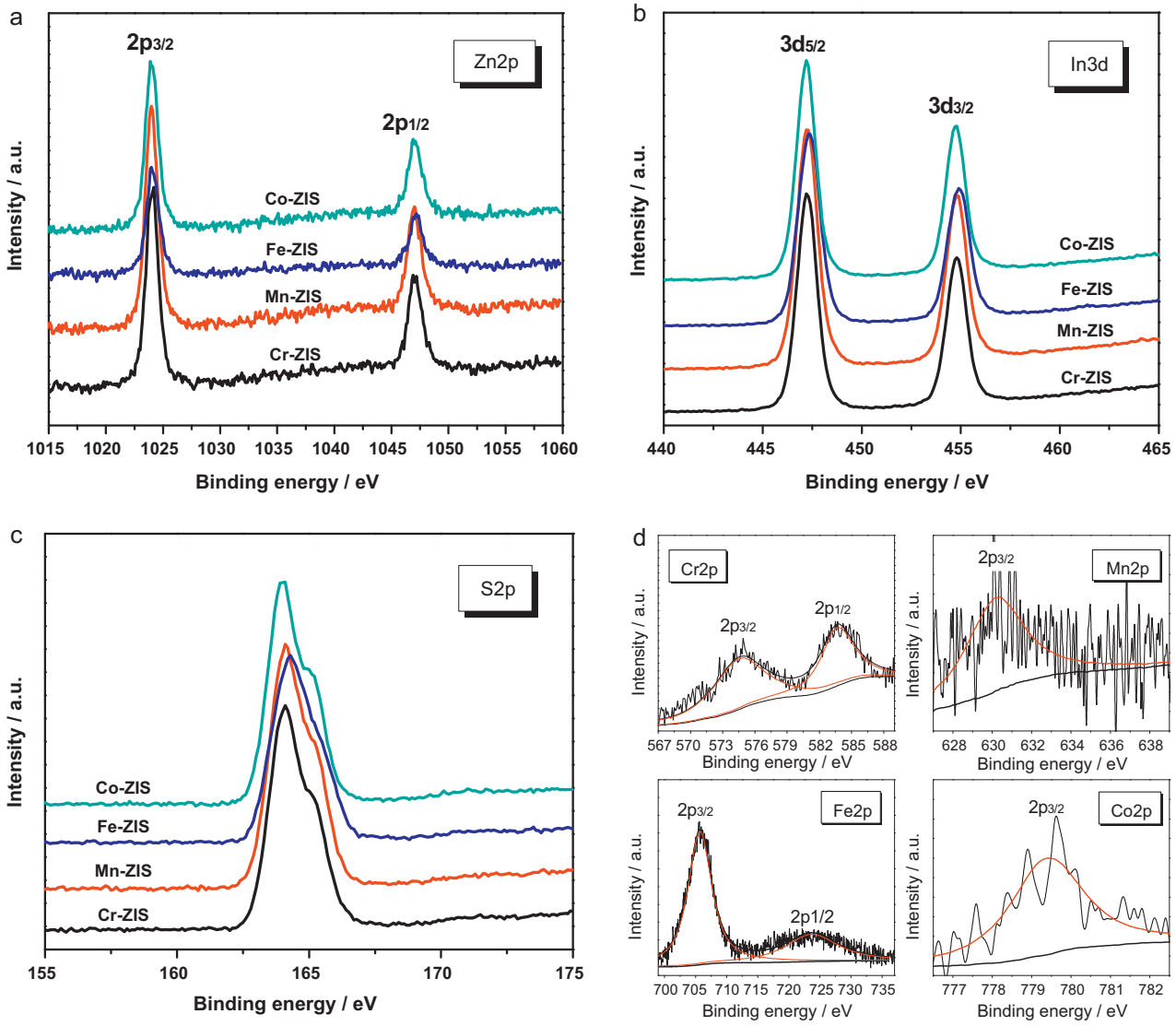

Fig. 3. XPS spectra of transition-metal doped $ZnIn_2S_4$ samples. (a) Zn2p spectra, (b) In3d spectra, (c) S2p spectra, and (d) Cr2p, Mn2p, Fe2p and Co2p spectra.

showed no appreciable H_2 evolution without irradiation or photocatalyst.

3. Results and discussion

3.1. X-ray diffraction and Raman spectra

Powder X-ray diffraction (XRD) and Raman spectra were used to determine the phase and crystal structure of the transition-metal doped $ZnIn_2S_4$ products (TM–ZIS, TM = Cr, Mn, Fe, Co).

Fig. 1 shows the XRD patterns of transition-metal doped $ZnIn_2S_4$ (TM–ZIS, TM = Cr, Mn, Fe, Co) as well as undoped $ZnIn_2S_4$ (ZIS). For ZIS, the intrinsic diffraction peaks, such as (0 0 6), (1 0 2), (1 0 4), (1 0 8), (1 1 2), (1 0 1 2), (2 0 2) and (2 1 3), can be readily indexed as the phase of hexagonal $ZnIn_2S_4$, as reported in our previous studies [17]. Moreover, impurities such as ZnS, In_2S_3, oxides or organic compounds related to reactants were hardly detected, indicating the purity of the undoped $ZnIn_2S_4$ sample. This demonstrates that $ZnIn_2S_4$ could be facilely synthesized during a short-time hydrothermal process under microwave assistance. When $ZnIn_2S_4$ was doped with transition-metal ions, the obtained TM–ZIS (TM = Cr, Mn, Fe, Co) samples exhibited almost the same XRD patterns as the undoped $ZnIn_2S_4$, as shown in Fig. 1(a). No characteristic peaks of the TM-contained compounds were found, implying that either transition-metal ions are incorporated in $ZnIn_2S_4$ lattice, or TM-contained compounds cannot be detected by XRD technique due to their small amounts and high dispersion. By carefully checking the (0 0 6) peak of TM–ZIS samples, we could find a small shift to higher angle occurs in the peak position after the introduction of transition metals. Table 1 shows the lattice parameters calculated from XRD results [23]. Compared to ZIS, the lattice

Table 1
Lattice parameters of transition-metal doped $ZnIn_2S_4$ samples derived from XRD patterns.

Samples	Lattice parameters (Å) [a]	
	a-axis	*c*-axis
ZIS	3.9635	26.8241
Cr–ZIS	3.9678	26.0677
Mn–ZIS	3.9537	26.1562
Fe–ZIS	3.9678	26.0236
Co–ZIS	3.9593	25.9944

[a] Calculated from the Bragg's Law, $2d_{hkl}\sin\theta = n\lambda$, and the formula for a hexagonal unit cell: $1/(d_{hkl})^2 = (4/3)\times(h^2+hk+k^2)/a^2 + l^2/c^2$. Here, d_{hkl} is the lattice spacing, (h, k, l) are the Miller indices, θ is the incident angle, n is an integer, λ is the wavelength of incident irradiation, and (a, c) are the lattice parameters.

parameters of TM–ZIS remain almost unchanged along the *a*-axis, whereas the *c*-axis parameters decrease as transition metal was doped, as shown in Fig. 1(b). Because of the smaller ionic radii of these transition metals than that of Zn^{2+} (0.74 Å) or In^{3+} (0.80 Å), *ex.* Cr^{3+} (0.62 Å), Mn^{2+} (0.67 Å), Fe^{3+} (0.55 Å) and Co^{2+} (0.65 Å) [24], it can be concluded that this crystal lattice distortion along *c*-axis is caused by the incorporation of transition-metal ions into the crystal lattice of $ZnIn_2S_4$. This means that transition-metal doping would influence the layered structure of hexagonal $ZnIn_2S_4$.

Fig. 2 shows the Raman spectra recorded under ambient conditions for transition-metal doped $ZnIn_2S_4$ (TM–ZIS, TM = Cr, Mn, Fe, Co) as well as undoped $ZnIn_2S_4$ (ZIS). The Raman spectra of all the samples are characterized by four Raman bands around 242, 300, 343 and 370 cm^{-1}, which could be assigned to the longitudinal optical mode (LO_1), transverse optical mode (TO_2), longitudinal optical mode (LO_2) and A_{1g} mode of $ZnIn_2S_4$, respectively. These results are in good agreement with the reported values for $ZnIn_2S_4$ [25,26]. The possible reason for the broadening of these Raman bands in TM–ZIS samples, especially the band around 300 cm^{-1}, should be the doping effects [27]. This also means the successful incorporation of transition-metal ions into the crystal lattice of $ZnIn_2S_4$. Additionally, no Raman bands due to TM-contained compounds can be observed in these TM–ZIS samples, which proves that transition-metal dopants are dispersed very well, and also confirms that transition-metal ions may be present in the substitutional positions in the lattice of $ZnIn_2S_4$.

3.2. XPS analysis

Fig. 3 shows the XPS spectra of transition-metal doped $ZnIn_2S_4$ samples. From the high-resolution XPS data of Zn2p, In3d, and S2p (Fig. 3(a–c)), we could easily find that the binding energies are in good agreement with the reported data of $ZnIn_2S_4$ in our previous literature [6]. The high-resolution Cr2p, Mn2p, Fe2p and Co2p XPS spectra of the TM–ZIS (TM = Cr, Mn, Fe, Co) samples are shown in Fig. 3(d). The binding energies of $Cr2p_{3/2}$, $Mn2p_{3/2}$, $Fe2p_{3/2}$ and $Co2p_{3/2}$ for TM–ZIS are at 474.7, 630.4, 705.8 and 779.4 eV, respectively. Furthermore, as listed in Table 2, the binding energies of $TM2p_{3/2}$ in TM–ZIS are lower than those in the corresponding transition-metal oxides (TM–O oxides), i.e., Cr_2O_3 [28], MnO [29], Fe_2O_3 [30] and CoO [31], respectively. For example, the $Fe2p_{3/2}$ binding energy in Fe(III)–S is lower than in Fe(III)–O [32]. This should be due to that TM–S bonds in the TM–ZIS samples are weaker than TM–O bonds in TM–O oxides, as sulfur is much less electronegative than oxygen. These results also confirm that the transition metals are incorporated into the lattice of $ZnIn_2S_4$ and form the TM–S bonds. The weight contents of these transition-metal dopants as given in Table 2 are very low, and that makes sure their successful incorporation in the lattice of $ZnIn_2S_4$.

3.3. UV–vis diffuse reflectance spectra and photoluminescence spectra

Fig. 4 shows the UV–vis diffuse reflectance spectra of transition-metal doped $ZnIn_2S_4$ samples (TM–ZIS, TM = Cr, Mn, Fe, Co) as well as undoped $ZnIn_2S_4$ (ZIS). As calculated from the onset of the absorption edge of ZIS at about 500 nm, the band gap is about 2.48 eV, which is quite close to the reported value in our previous studies [17,20]. When transition-metal ions are doped into the lattice of $ZnIn_2S_4$, a red shift in UV–vis absorption band occurs in the spectra of TM–ZIS. This is resulted from the impurity energy levels created in the forbidden band of ZIS by transition-metal doping, which narrows the band gap of TM–ZIS. Deduced from the previous results on the calculated band structures of transition-metal (TM = Cr, Mn, Fe, Co) doped ZnS [33], the localized states contributed by the TM-3d valence electrons would introduce

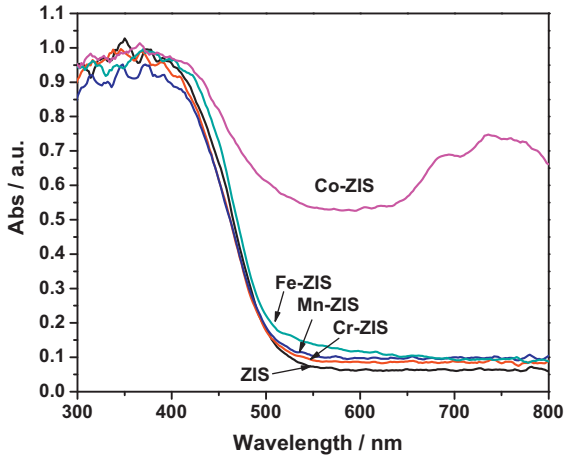

Fig. 4. UV–vis diffuse reflectance spectra of transition-metal doped $ZnIn_2S_4$ samples.

occupied states in the gap region of $ZnIn_2S_4$ and then give rise to the narrower band gap of TM–ZIS. Moreover, the TM-3d orbitals are proposed to decompose into two parts, t_{2g} state in the lower energy region and e_g state in the higher energy region [34]. For example, the absorption tail in the range of 500–700 nm for Fe–ZIS might be due to the split Fe-3d orbitals formed in the gap of $ZnIn_2S_4$. One should have noted that Co–ZIS strongly absorbs the visible light photons with wavelength longer than 500 nm, which should be attributed to the absorption transition related to the discrete suborbitals further split from Co-3d t_{2g} and e_g states. As reported in some Co-contained oxide compounds, the Co-3d e_g orbital further split into a higher-energy $d_{x^2-y^2}$ orbital and a lower-energy d_{z^2} orbital, while the Co-3d t_{2g} orbital further split into three discrete suborbitals: d_{xy}, d_{yz}, and d_{xz} [35].

Fig. 5 shows the photoluminescence spectra of transition-metal doped $ZnIn_2S_4$ samples (TM–ZIS, TM = Cr, Mn, Fe, Co) as well as undoped $ZnIn_2S_4$ (ZIS). The photoluminescence properties of TM–ZIS were influenced by TM doping. For ZIS, the emission peak around 560 nm should be due to the band-to-band transition. However, this emission peak of ZIS is about 60 nm red-shifted vs. the absorption edge. Such red-shift also occurs in the emission spectra of TM–ZIS (TM = Cr, Mn, Fe), when compared with their UV–vis spectra as shown in Fig. 4. A similar phenomenon has been previously reported on Cu-doped $ZnIn_2S_4$, due to the broadband or donor-acceptor defect (such as sulfur vacancy) based photoluminescence emission of $ZnIn_2S_4$ or doped $ZnIn_2S_4$ [20]. By further checking the photoluminescence spectra of Cr–ZIS and Co–ZIS, we

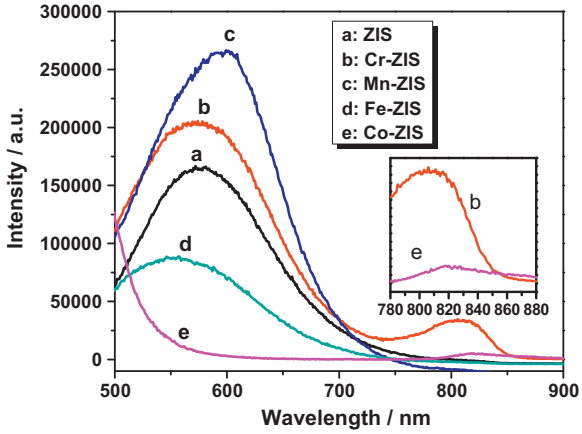

Fig. 5. Photoluminescence spectra of transition-metal doped $ZnIn_2S_4$ samples.

Table 2
XRF and XPS results of transition-metal doped $ZnIn_2S_4$ samples.

Samples	Dopant	Weight content[a] (%)	Element transition	Binding energy[b] (eV)	Referenced binding energy[c] (eV)
Cr–ZIS	Cr^{3+}	0.08	Cr $2p_{3/2}$	574.7	576.6 [28]
Mn–ZIS	Mn^{2+}	0.03	Mn $2p_{3/2}$	630.4	640.4 [29]
Fe–ZIS	Fe^{3+}	0.28	Fe $2p_{3/2}$	705.8	710.9 [30]
Co–ZIS	Co^{2+}	0.42	Co $2p_{3/2}$	779.4	780.6 [31]

[a] Calculated from XRF analysis results.
[b] Obtained from XPS analysis.
[c] Obtained from transition-metal oxides, Cr_2O_3, MnO, Fe_2O_3 and CoO, respectively.

could find a second emission peak around 810 nm and 820 nm, respectively. This emission transition could be explained by the splitting of Cr-3d and Co-3d orbitals created in the forbidden band, thus attributed to the d-d transition between the split Cr-3d and Co-3d orbitals, respectively. Though the splitting of Cr-3d orbitals is not reflected in the UV–vis spectra of Cr–ZIS due to the small amount of Cr doping, the fact that Cr-3d orbitals split to t_{2g} and e_g states could be expected [36].

Again, we take the emission peak around 560 nm into discussion, as the photoluminescence intensity was reported to affect the photocatalytic activity greatly [20]. After Cr and Mn doping, the photoluminescence intensity for TM–ZIS (TM = Cr, Mn) is enhanced in the order of ZIS < Cr–ZIS < Mn–ZIS. This should contribute to the band gap narrowed by Cr and Mn doping, which gives rise to the larger amounts of photogenerated electrons and holes and hence the enhanced photoluminescence intensity of band-to-band transition. Additionally, Cr and Mn doping would introduce more defect states (e.g., sulfur vacancy), which also results in the enhanced photoluminescence intensity, as the foregoing analysis showing such photoluminescence emission was related to native defects [20]. However, after Fe and Co doping, the photoluminescence intensity for TM–ZIS (TM = Fe, Co) is decreased in the order of ZIS > Fe–ZIS > Co–ZIS. Especially for Co–ZIS, one cannot find any emission peak around 560 nm. It was reported that Fe and Co doping had a quenching effect on the photoluminescence intensity [37,38]. The discrete energy levels introduced by Fe and Co doping as discussed above could act as electron trapping centers which results in non-radiative recombination [37,38]. Here, it is worth noting that such non-radiative recombination or transition is detrimental to photocatalytic activity, which will be discussed later.

Taking into account the above-mentioned photophysical and optical properties, the band structures of transition-metal doped $ZnIn_2S_4$ samples (TM–ZIS, TM = Cr, Mn, Fe, Co) and undoped $ZnIn_2S_4$ (ZIS) are schematically illustrated in Fig. 6. Our previous band calculation results demonstrate that the highest occupied molecular orbital (HOMO) levels and the lowest unoccupied molecular orbital (LUMO) levels of $ZnIn_2S_4$ are composed mainly of the hybridized S3p and Zn3d orbitals, and the In5s5p and S3p orbitals, respectively [20]. Upon photoexcitation, electron will transfer from valence band to conduction band of $ZnIn_2S_4$, while photoluminescence emission could be due to the transition from conduction band and sulfur vacancy related donor level to valence band. After transition metal doping, the impurity levels of TM-3d e_g and t_{2g} states will form in the gap of $ZnIn_2S_4$. For Cr–ZIS and Mn–ZIS, the impurity levels will reduce the band gap and introduce more defect states (e.g., sulfur vacancy). That's why their photoluminescence intensities of defect-related band-to-band transition with emission around 560 nm were enhanced. The d–d transition from Cr-3d e_g state to t_{2g} state should contribute to the additional photoluminescence emission around 810 nm for Cr–ZIS. For Fe–ZIS and Co–ZIS, although the band gaps were reduced by Fe and Co doping, the intensity of photoluminescence emission related to band-to-band transition was decreased due to the split TM-3d e_g and t_{2g} orbitals (TM = Fe, Co) acting as non-radiative recombination centers for photoinduced electrons and holes.

3.4. SEM analysis

Fig. 7 shows SEM images for transition-metal doped $ZnIn_2S_4$ samples (TM–ZIS, TM = Cr, Mn, Fe, Co) as well as undoped $ZnIn_2S_4$ (ZIS). Without transition-metal doping, ZIS displays the morphology of separate microclusters composed of numerous petals/sheets. This growth tendency of lamellar structures is related to the layered feature of hexagonal $ZnIn_2S_4$. However, when compared to the microsphere-shaped $ZnIn_2S_4$ synthesized by hydrothermal method [20], the ZIS sample turns to be much more irregular. This might be because the microwave irradiation hinders the formation of regular microsphere in hydrothermal condition. All the TM–ZIS samples also display the morphology of petal/sheet-composed microclusters similar to ZIS. Thus, it could be concluded that the small amount doping will not destroy the initial morphology of ZIS, according to the reported fact that large amount of Cu^{2+} doping destructed the initial morphology and layered structure of $ZnIn_2S_4$, whereas small amount of Cu^{2+} doping would not [20]. Moreover, excessive transition-metal ion doping will form impurity phases acting as recombination centers of photoinduced electrons and holes [20,39]. This always greatly lowers down the photocatalytic activity of doped semiconducting materials. Therefore, in this study, small amounts of transition-metal ions were chosen to dope into $ZnIn_2S_4$ to prevent the possible formation of impurity phase induced by excessive dopants.

3.5. Photocatalytic activity

Fig. 8 shows the rate of photocatalytic hydrogen evolution and time course of hydrogen evolution over transition-metal doped $ZnIn_2S_4$ (TM–ZIS, TM = Cr, Mn, Fe, Co) under visible light irradiation. Either ZIS or TM–ZIS is active for splitting water to hydrogen. For all samples, the amount of evolved H_2 (μmol) after 6 h far exceeds the amount of catalyst (about 23.6 μmol), indicating that the reaction occurs catalytically. The rate of H_2 evolution over ZIS is about 104.0 μmol h^{-1}. It is clear that Mn–ZIS shows better photocatalytic hydrogen production performance, with rate of hydrogen evolution 20% higher than ZIS, and total amount of generated hydrogen increases very steadily without apparent change during a testing course of 6 h, suggesting its good photocatalytic stability. However, the evolution rate of H_2 decreases in other TM–ZIS samples, with an order of ZIS > Cr–ZIS > Fe–ZIS > Co–ZIS. As shown in Fig. 8(a), Cr, Fe and Co as the dopants shows negative or neutral effect on the hydrogen evolution reaction, while only Mn doping has a slight positive effect (only 20% enhancement) on the photocatalytic activity of $ZnIn_2S_4$. Therefore, the following studies on Mn-doped $ZnIn_2S_4$, such as the effects of Mn doping amounts on the photocatalytic activity, are necessary for the further improvement on photocatalytic hydrogen evolution over doped $ZnIn_2S_4$.

From the results of XRD and SEM analysis, the crystal structure and morphology should not be the main reasons for the different

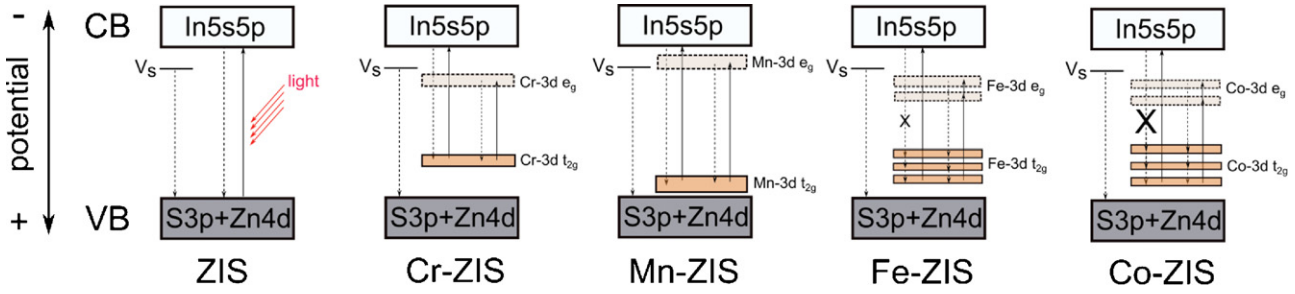

Fig. 6. Schematic band structures of undoped $ZnIn_2S_4$ and transition-metal doped $ZnIn_2S_4$. CB and VB stand for conduction band and valence band, respectively. V_s Stands for sulfur vacancy. Solid arrows and dotted arrows represent photoexcitation and photoluminescence transition, respectively. Cross (×) implies photoluminescence quenching.

effects of transition metals (Cr, Mn, Fe, Co) on photocatalytic activity, as all the doped $ZnIn_2S_4$ have similar crystal structure and morphology. Therefore, it is interesting to explore the possible reasons for the different effects of transition-metal doping on the photocatalytic activity of $ZnIn_2S_4$ from other aspects of their inherent properties such as band structure. It is generally accepted that the smaller the band gap and hence the larger the number of absorbed photons, the higher is the photocatalytic activity of a photocatalyst. As known from the UV–vis spectra in Fig. 4 and band structures of TM–ZIS in Fig. 6, all the TM–ZIS samples have narrower band gap than ZIS. However, only the Mn–ZIS sample displays higher photocatalytic activity than ZIS, due to the

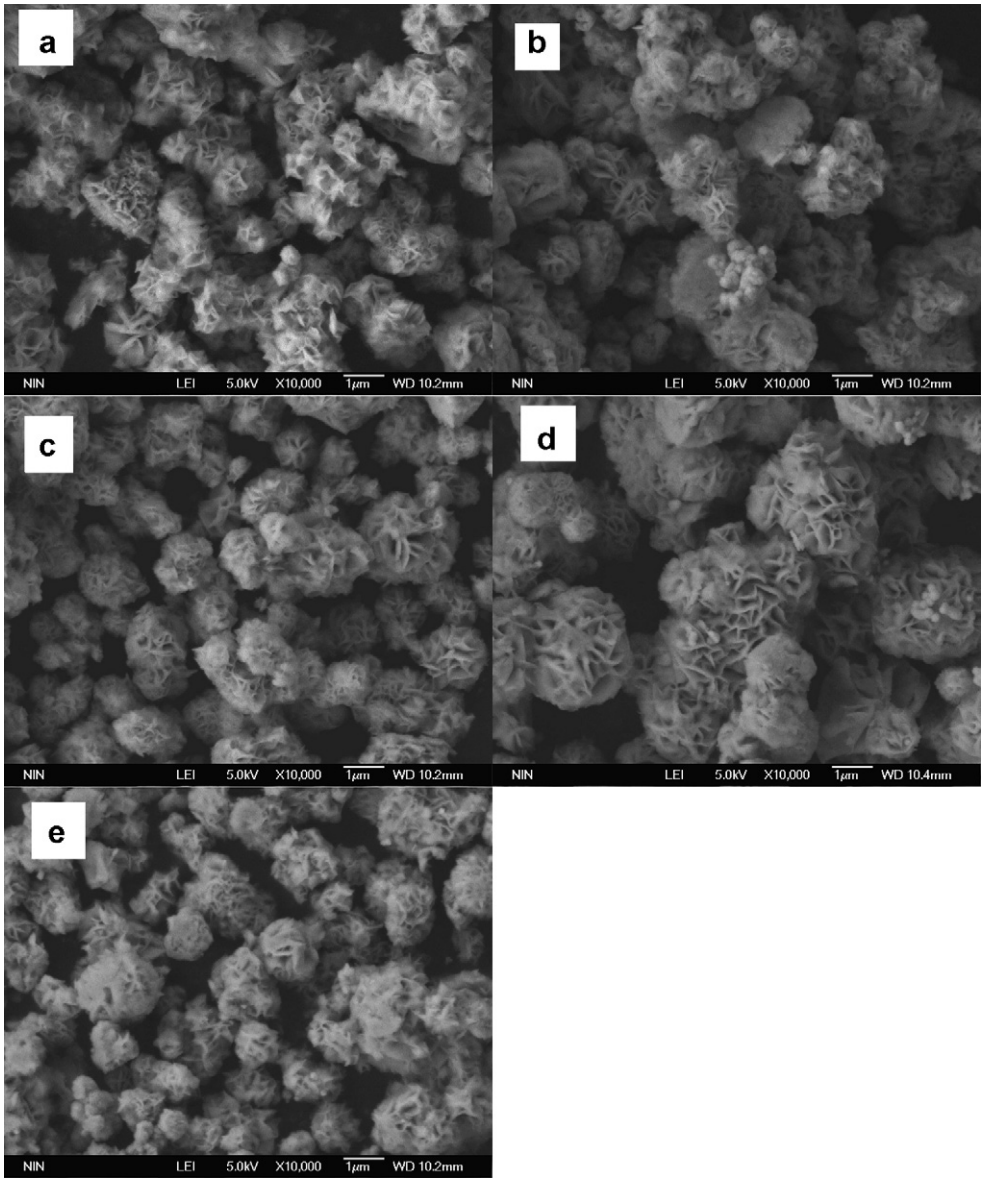

Fig. 7. SEM images of transition-metal doped $ZnIn_2S_4$ samples. (a) ZIS, (b) Cr–ZIS, (c) Mn–ZIS, (d) Fe–ZIS, and (e) Co–ZIS.

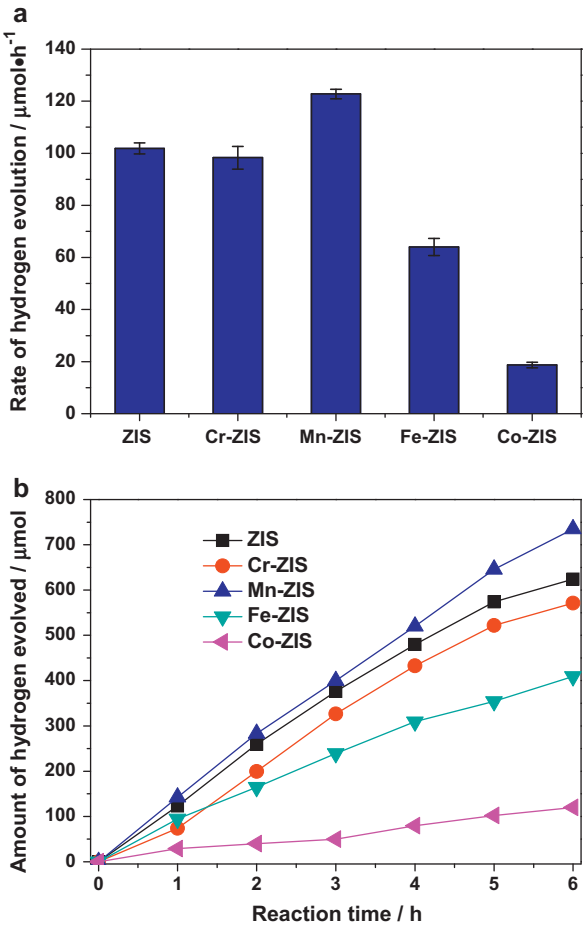

Fig. 8. Photocatalytic hydrogen evolution rates (a) and time courses of hydrogen evolution (b) over transition-metal doped $ZnIn_2S_4$ samples under visible light irradiation.

narrowed band gap by Mn doping. Thus, it could be deduced that there should be some other key factors derived from their different band structures contributing to the different effects of TM-doping on photocatalytic activity.

When looking into the case of Cr–ZIS, worse photocatalytic activity than ZIS was performed, though more photoexcited electrons were generated in Cr–ZIS as indicated by its narrowed band gap and enhanced photoluminescence emission intensity of band-to-band transition. This might be because the discrete energy levels introduced by Cr doping in the gap of $ZnIn_2S_4$ as depicted in Fig. 6 would localize the charge carriers and hinder charge transfer to catalyst surface for reaction, and then suppress the photocatalytic activity of Cr–ZIS. Such deactivation of photocatalytic hydrogen production by Cr doping was also reported on some other photocatalysts [34]. For Mn–ZIS, Mn-3d e_g state and t_{2g} state, which lie slightly above the valence band and below the conduction band, respectively, play the role in narrowing the band gap of $ZnIn_2S_4$ and hence enhance the photocatalytic activity. Moreover, the Mn-3d level (t_{2g} here) could serve as shallow trapping sites for holes and thus separate electron-hole pairs for the promoted photocatalytic reaction [40].

As reported previously, if non-radiative transition dominates in a photocatalyst, the number of electrons and holes to be involved in the photocatalytic reaction is decreased, which results in a decrease in the photocatalytic activity [41]. As discussed on the photoluminescence spectra and band structures in the earlier sections, compared to undoped $ZnIn_2S_4$, the emission intensities of band-to-band transition for Fe–ZIS and Co–ZIS decrease due to the photoluminescence quenching effect of Fe and Co doping by introducing impurity energy levels acting as non-radiative recombination centers. Such photoluminescence quenching results in the decreased emission intensity in the order of ZIS > Fe–ZIS > Co–ZIS, which means the number of electrons and holes available for photocatalytic reaction decreases in the order of ZIS > Fe–ZIS > Co–ZIS. Thus, it is reasonable that the photocatalytic activity for hydrogen evolution decreases in the order of ZIS > Fe–ZIS > Co–ZIS.

Consequently, based on the different band structures of TM–ZIS (TM = Cr, Mn, Fe, Co) samples and the analysis results of UV–vis absorption spectra and photoluminescence spectra, the different effects of transition-metal doping on photocatalytic activity could be explained briefly as follows: For Mn–ZIS, the critical factor for enhanced photocatalytic activity should be possibly due to the narrowed band gap and promoted charge separation by Mn doping. For TM–ZIS (TM = Cr, Fe, Co), the limiting factor for decreased photocatalytic activities maybe lies in the reduced numbers of electrons and holes available for photocatalytic reaction, which is induced by localization of charge carriers at discrete energy levels introduced by Cr doping, and non-radiative recombination of electrons and holes at impurity energy levels introduced by Fe and Co doping, respectively.

4. Conclusions

In summary, a series of transition-metal (Cr, Mn, Fe, Co) doped $ZnIn_2S_4$ photocatalysts was prepared by a facile microwave-assisted hydrothermal method. The transition metals were successfully incorporated into the lattices of $ZnIn_2S_4$, as proved by XRD, Raman and XPS analysis results. When compared to undoped $ZnIn_2S_4$, the Mn-doped $ZnIn_2S_4$ showed photocatalytic activity enhanced for hydrogen evolution under visible light, whereas, the Cr-, Fe-, Co-doped $ZnIn_2S_4$ displayed suppressed photocatalytic activities. It is assumed that the impurity energy levels introduced in the gap of $ZnIn_2S_4$ by transition-metal doping have different effects on photocatalytic performances, although the visible-light absorption ranges of all the doped $ZnIn_2S_4$ were expanded. For Mn-doped $ZnIn_2S_4$, the enhancement of photocatalytic activity could be due to the increased number of electrons and holes for photocatalytic reaction induced by Mn doping. However, for Cr-, Fe-, and Co-doped $ZnIn_2S_4$, the impurity energy levels created in the gap of $ZnIn_2S_4$ by transition-metal doping could localize the charge carriers or act as non-radiative recombination centers for photoexcited electrons and holes. This led to their lower photocatalytic activities for hydrogen evolution than undoped $ZnIn_2S_4$. As a summary of this study, all the dopants tested showed a negative or neutral effect on the hydrogen evolution reaction, with the possible exception of Mn, and in that case further studies are warranted.

Acknowledgements

The authors gratefully acknowledge the financial supports of the National Natural Science Foundation of China (No. 51102194 and No. 91010012), National Basic Research Program of China (No. 2009CB220000) and Natural Science Foundation of Shaanxi Province (No. 2011JQ7017). One of the authors (SS) was supported by “the Fundamental Research Funds for the Central University”.

References

[1] A. Fujishima, K. Honda, Nature 238 (1972) 37–38.
[2] X. Chen, S. Shen, L. Guo, S.S. Mao, Chem. Rev. 110 (2010) 6503–6570.
[3] S. Shen, J. Shi, P. Guo, L. Guo, Int. J. Nanotechnol. 8 (2011) 523–590.
[4] Z. Chen, D. Li, W. Zhang, Y. Shao, T. Chen, M. Sun, X. Fu, J. Phys. Chem. C 113 (2009) 4433–4440.

[5] Y. Chen, S. Hu, W. Liu, X. Chen, L. Wu, X. Wang, P. Liu, Z. Li, Dalton Trans. 40 (2011) 2607–2613.
[6] S. Shen, L. Zhao, L. Guo, J. Phys. Chem. Solids 69 (2008) 2426–2432.
[7] S. Shen, L. Zhao, L. Guo, Int. J. Hydrogen Energy 35 (2010) 10148–10154.
[8] I. Tsuji, H. Kato, H. Kobayashi, A. Kudo, J. Am. Chem. Soc. 126 (2004) 13406–13413.
[9] I. Tsuji, H. Kato, A. Kudo, Angew. Chem. Int. Ed. 44 (2005) 3565–3568.
[10] Y. Li, G. Chen, C. Zhou, J. Sun, Chem. Commun. 15 (2009) 2020–2022.
[11] Y. Li, G. Chen, Q. Wang, X. Wang, A. Zhou, Z. Shen, Adv. Funct. Mater. 22 (2010) 3390–3398.
[12] J.S. Jang, S.H. Choi, N. Shin, C. Yu, J.S. Lee, J. Solid State Chem. 180 (2007) 1110–1118.
[13] J.S. Jang, P.H. Borse, J.S. Lee, S.H. Choi, H.G. Kim, J. Chem. Phys. 128 (2008) 154717.
[14] M. Tabata, K. Maeda, T. Ishihara, T. Minegishi, T. Takata, K. Domen, J. Phys. Chem. C 114 (2010) 11215–11220.
[15] H. Kaga, K. Saito, A. Kudo, Chem. Commun. 46 (2010) 3779–3781.
[16] Z. Lei, W. You, M. Liu, G. Zhou, T. Takata, M. Hara, K. Domen, C. Li, Chem. Commun. 17 (2003) 2142–2143.
[17] S. Shen, L. Zhao, L. Guo, Int. J. Hydrogen Energy 33 (2008) 4501–4510.
[18] S. Shen, L. Zhao, L. Guo, Mater. Res. Bull. 44 (2009) 100–105.
[19] S. Shen, X. Chen, F. Ren, C.X. Kronawitter, S.S. Mao, L. Guo, Nanoscale Res. Lett. 6 (2011) 290–295.
[20] S. Shen, L. Zhao, Z. Zhou, L. Guo, J. Phys. Chem. C 112 (2008) 16148–16155.
[21] D. Jing, M. Liu, L. Guo, Catal. Lett. 140 (2010) 167–171.
[22] M. Sun, D. Li, Y. Zheng, W. Zhang, Y. Shao, Y. Chen, W. Li, X. Fuv, Environ. Sci. Technol. 43 (2009) 7877–7882.
[23] V.K. Pecharsky, P.Y. Zavalij, Fundamentals of Powder Diffraction and Structural Characterization of Materials, Springer, New York, 2009.
[24] R.D. Shannon, Acta Crystallogr. A 32 (1976) 751–767.
[25] G. Baldini, R.L. Aggarwal, B. Lax, S.H. Shin, J.C. Tsang, Lett. Nuovo Cimento 5 (1972) 1062–1066.
[26] W.K. Unger, B. Farnworth, J.C. Irwin, H. Pink, Solid State Commun. 25 (1978) 913–915.
[27] C. Bi, L. Pan, M. Xu, J. Yin, Z. Guo, L. Qin, H. Zhu, J.Q. Xiao, Chem. Phys. Lett. 481 (2009) 220–223.
[28] M. Hassel, I. Hemmerich, H. Kuhlenbeck, H.-J. Freund, Surf. Sci. Spectra 4 (1996) 246–252.
[29] H.W. Nesbitt, D. Banerjee, Am. Mineral. 83 (1998) 305–315.
[30] T. Fujii, F.M.F. de Groot, G.A. Sawatzky, F.C. Voogt, T. Hibma, K. Okada, Phys. Rev. B 59 (1999) 3195–3202.
[31] M. Hassel, H.-J. Freund, Surf. Sci. Spectra 4 (1996) 273–278.
[32] S. Boursiquot, M. Mullet, J.-J. Ehrhardt, Surf. Interface Anal. 34 (2002) 293–297.
[33] H. Chen, D. Shi, J. Qi, J. Appl. Phys. 109 (2011) 084338.
[34] J. Ye, Z. Zou, J. Phys. Chem. Solids 66 (2005) 266–273.
[35] J. Yin, Z. Zou, J. Ye, J. Phys. Chem. B 107 (2003) 4936–4941.
[36] D. Wang, J. Ye, H. Kitazawa, T. Kimura, J. Phys. Chem. C 111 (2007) 12848–12854.
[37] P.H. Borse, N. Deshmukh, R.F. Shinde, S.K. Date, S.K. Kulkarni, J. Mater. Sci. 34 (1999) 6087–6093.
[38] H.A. Weakliem, J. Chem. Phys. 36 (1962) 2117–2140.
[39] I. Tsuji, A. Kudo, J. Photochem. Photobiol. A: Chem. 156 (2003) 249–252.
[40] M. Liu, Y. Du, L. Ma, D. Jing, L. Guo, Int. J. Hydrogen Energy (2011), doi:10.1016/j.ijhydene.2011.04.111.
[41] Y. Yuan, Z. Zhao, J. Zheng, M. Yang, L. Qiu, Z. Li, Z. Zou, J. Mater. Chem. 20 (2010) 6772–6779.